Journal of Medicinal Chemistry

Article

Novel, Highly Potent Adenosine Deaminase Inhibitors Containing the Pyrazolo[3,4-*d*]pyrimidine Ring System. Synthesis, Structure–Activity Relationships, and Molecular Modeling Studies

Federico Da Settimo, Giampaolo Primofiore, Concettina La Motta, Sabrina Taliani, Francesca Simorini, Anna Maria Marini, Laura Mugnaini, Antonio Lavecchia, Ettore Novellino, Daniela Tuscano, and Claudia Martini

J. Med. Chem., **2005**, 48 (16), 5162-5174• DOI: 10.1021/jm050136d • Publication Date (Web): 09 July 2005

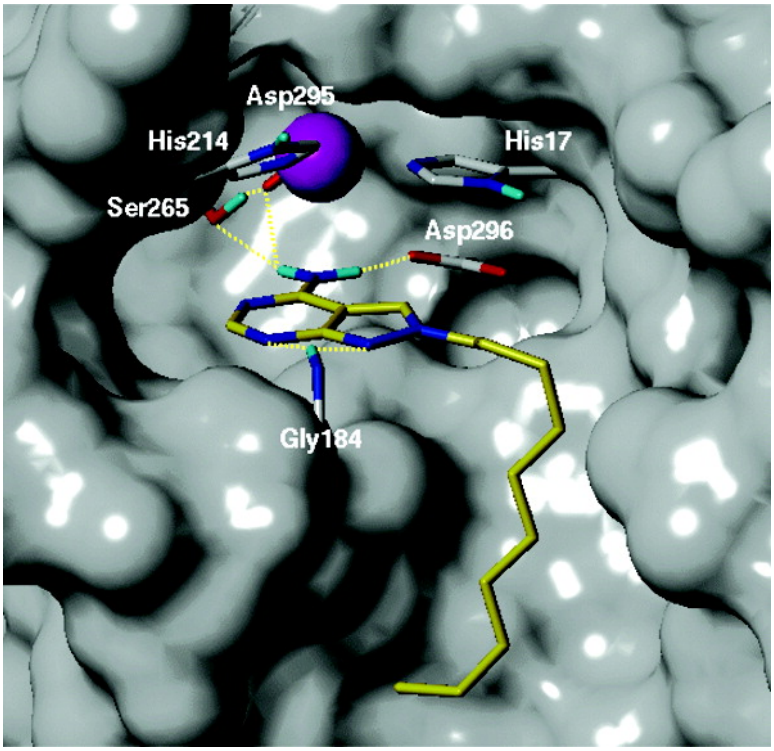

More About This Article

Additional resources and features associated with this article are available within the HTML version:

- Supporting Information
- Links to the 5 articles that cite this article, as of the time of this article download
- Access to high resolution figures

Journal of Medicinal Chemistry is published by the American Chemical Society. 1155 Sixteenth Street N.W., Washington, DC 20036

Novel, Highly Potent Adenosine Deaminase Inhibitors Containing the Pyrazolo[3,4-*d*]pyrimidine Ring System. Synthesis, Structure−Activity Relationships, and Molecular Modeling Studies

Federico Da Settimo,[†] Giampaolo Primofiore,[†] Concettina La Motta,*[,†] Sabrina Taliani, Francesca Simorini, Anna Maria Marini, Laura Mugnaini,[†] Antonio Lavecchia,*[,§] Ettore Novellino,[§] Daniela Tuscano,[‡] and Claudia Martini[‡]

Dipartimento di Scienze Farmaceutiche, Università di Pisa, Via Bonanno 6, 56126 Pisa, Italy, Dipartimento di Chimica Farmaceutica e Tossicologica, Università di Napoli "Federico II", Via D. Montesano, 49, 80131 Napoli, Italy, and Dipartimento di Psichiatria, Neurobiologia, Farmacologia e Biotecnologie, Università di Pisa, Via Bonanno 6, 56126 Pisa, Italy

Received February 11, 2005

This study reports the synthesis of a number of 1- and 2-alkyl derivatives of the 4-aminopyrazolo[3,4-*d*]pyrimidine (APP) nucleus and their evaluation as inhibitors of ADA from bovine spleen. The 2-substituted aminopyrazolopyrimidines proved to be potent inhibitors, most of them exhibiting K_i values in the nanomolar/subnanomolar range. In this series the inhibitory activity is enhanced with the increase in length of the alkyl chain, reaching a maximum with the *n*-decyl substituent. Insertion of a 2′-hydroxy group in the *n*-decyl chain gave **3k**, whose (*R*)-isomer displayed the highest inhibitory potency of the series (K_i 0.053 nM), showing an activity 2 orders of magnitude higher than that of (+)-EHNA (K_i 1.14 nM), which was taken as the reference standard. Docking simulations of aminopyrazolopyrimidines into the ADA binding site were also performed, to rationalize the structure−activity relationships of this class of inhibitors.

Introduction

Adenosine deaminase (ADA, EC 3.5.4.4) is a catabolic enzyme of purine metabolism that catalyzes the irreversible deamination of adenosine and 2′-deoxyadenosine to inosine and 2′-deoxyinosine, respectively. It is a ubiquitous enzyme which regulates the levels of endogenous adenosine and, in addition, plays a central role in the differentiation and maturation of the lymphoid system.[1] ADA has been the object of considerable interest mainly because its congenital defect in human beings causes severe combined immunodeficiency disease (SCID), in which both B-cell and T-cell development is impaired. Actually, SCID is caused by a high concentration of 2′-deoxyadenosine-5′-triphosphate (dATP), which is lymphotoxic; consequently ADA inhibition may be useful for the selective treatment of lymphoproliferative malignancies.[2−5] Indeed, the ability of the two natural strong ADA inhibitors coformycin[6] (CF, **I**) and 2′-deoxycoformycin[7] (dCF, pentostatin, **II**, Chart 1) to mimic ADA deficiency has been associated with their potent antitumor properties, since they should act as immunosuppressants to control cancers of the hyperimmune system, such as leukemia and lymphoma. ADA inhibition may also be used to prevent deamination and subsequent deactivation of adenine-containing chemotherapeutic agents such as 8-aza-adenosine, arabinofuranosyladenine (ara-A), or formycin A, thus potentiating their therapeutic activity.[8,9] Furthermore, as both cerebral and myocardial ischemia result in the release of adenosine which appears to limit the extent of degeneration, another potential use of ADA inhibitors is that of protective agents in these events.[10−13]

Chart 1

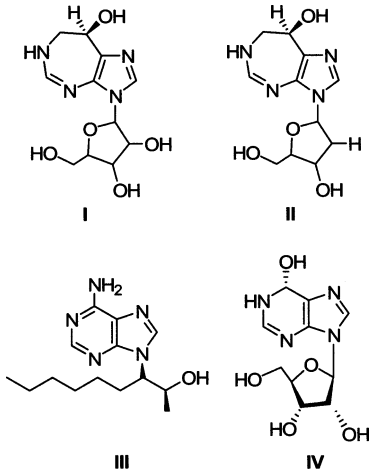

Certainly, inhibition of ADA will inevitably be a nonselective treatment, as it will stimulate all adenosine receptor subtypes; thus, to minimize undesiderable side effects, ADA inhibitors have to be selective for the enzyme without interfering with adenosine receptors, which could lead to the alteration of the physiology of many organ systems. Due to this wide therapeutic potential, there is a continuous interest in the development of new ADA inhibitors.

Potent ADA inhibitors may be divided into two classes, which are called ground-state inhibitors if their

* To whom all correspondence should be addressed. C.L.M.: Tel: (+39)0502219547; Fax: (+)390502219605; E-mail: lamotta@farm.unipi.it. A.L.V.: Tel and Fax: (+39)081678613; E-mail: lavecchi@unina.it.

[†] Dipartimento di Scienze Farmaceutiche, Università di Pisa.

[§] Dipartimento di Chimica Farmaceutica e Tossicologica, Università "Federico II" di Napoli.

[‡] Dipartimento di Psichiatria, Neurobiologia, Farmacologia e Biotecnologie, Università di Pisa.

10.1021/jm050136d CCC: $30.25
Published on Web 07/09/2005

Scheme 1

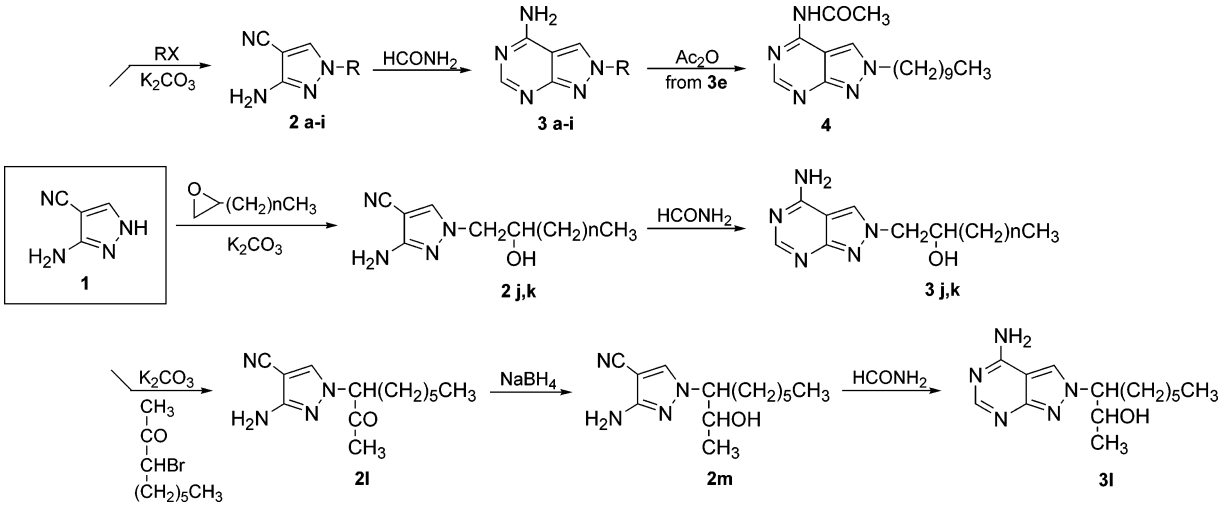

structure is similar to that of the endogenous ADA substrate adenosine, and transition-state inhibitors when their structure resembles that of the tetrahedral transition-state intermediate which forms during the deamination process catalyzed by the enzyme. Erythro-9-(2-hydroxy-3-nonyl)adenine[14] (EHNA, **III**, Chart 1) and 2′-deoxycoformycin (dCF, **II**, Chart 1) are the most potent examples of the first and the second classes, respectively. dCF is so tightly bound to the enzyme (K_i 2.5×10^{-3} nM) that its inhibitory action is nearly irreversible. The toxicity observed with dCF therapy seems to be principally due to the prolonged inhibition of ADA, leading to immunosuppressive effects. On the other hand, the rapid metabolism of EHNA allows a fast recovery of the enzyme activity, with poor therapeutic effects. Thus, it is believed that attractive inhibitors would be analogues that are 1−2 orders of magnitude more potent than EHNA.

These observations greatly stimulated our interest in discovering EHNA analogues in which the adenine base was substituted by the 4-aminopyrazolo[3,4-*d*]-pyrimidine (APP) system bearing alkyl, arylalkyl, or hydroxyalkyl chains in positions 1 or 2 (compounds **3a**−**l** and **12a**−**f**,**h**,**i**, respectively). Actually, the pyrazolo[3,4-*d*]pyrimidine nucleus proved to be a suitable scaffold for adenosine antagonists and of inhibitors of another purine metabolism enzyme, namely adenosine kinase.[15−20] Moreover, this scaffold, which offered the possibility of substituting two different positions (1 and 2), appeared to be particularly versatile to investigate the structural requirements of the ADA catalytic site. To better delineate the structure−activity relationships (SARs) of this new class of ADA inhibitors, the 6-phenyl derivative **13** of the most potent compound **3e** was also prepared and tested, since it has been reported[21] that a 2-phenyl group increases the binding of EHNA toward ADA. Finally, to verify if also for this class of inhibitors, as for 9-alkyladenines, substitution at the hexocyclic amino group was detrimental for inhibitory activity,[22] the N^4-acetyl derivative **4** was synthesized and tested.

As several products of this study presented a chiral center (**3j**, **3k**, **3l**, **12f**, and **12h**), a preliminary biological evaluation was conducted on their stereoisomeric mixtures, to identify the racemate with the best ability to inhibit the enzyme. Derivative **3k** (K_i 0.28 nM) showed the highest potency for ADA inhibition among this set of compounds. The synthesis of both *R* and *S* isomers of **3k** was therefore undertaken, to investigate how their potency is affected by the stereochemistry at the hydroxyl-bearing β-carbon, as occurs for the 9-(2-hydroxy-3-nonyl) side chain of EHNA.

The crystal structure of a murine ADA complexed with 6-hydroxy-1,6-dihydropurine ribonucleoside[23] (HDPR, **IV**, Chart 1), a tight-binding transition-state inhibitor, was determined at 2.4 Å resolution. However, no similar data are available for a semi-tight-binding inhibitor such as EHNA; neither the conformation nor its binding site have been fully elucidated yet. Thus, docking simulations of our very potent inhibitor **3e** together with (*R*)- and (*S*)-isomers of **3k**, and EHNA, were performed, both to rationalize the SARs observed and to gain more information about the ADA catalytic site.

Chemistry

The synthesis of the N^2-substituted pyrazolo[3,4-*d*]-pyrimidines **3a**−**l** and **4** was performed starting from the commercially available 3-amino-4-pyrazolecarbonitrile **1**, as illustrated in Scheme 1. Alkylation of **1** with the suitable reactants in DMF at 100 °C, in the presence of K_2CO_3, gave the N^1-alkylpyrazoles **2a**−**l** as the main reaction products. In particular, treatment of **1** with the appropriate alkyl bromides led to compounds **2a**−**i**, reaction with 1,2-epoxyoctane, 1,2-epoxydecane, and (*R*)-(+)- and (*S*)-(−)-1,2-epoxydecane provided the alcohols **2j**, **2k**, and (*R*)-**2k** and (*S*)-**2k**, respectively, and alkylation with 3-bromononan-2-one[24] gave the pyrazole **2l**, which, after reduction with $NaBH_4$ in methanolic solution at room temperature, afforded the intermediate **2m**, bearing the EHNA side chain.

Cyclization of **2a**−**k**,**m** with boiling formamide provided the desired inhibitors **3a**−**l**. The acetylamino derivative **4** was obtained with a good yield upon treatment of a pyridine solution of **3e** with acetic anhydride at 100 °C. The (*S*)-(−)-1,2-epoxydecane used to obtain enantiomerically pure (*S*)-**3k** was prepared from the commercially available (*R*)-(+)-1,2-decanediole **5** in the four-step sequence outlined in Scheme 2, which involved an inversion at C2. Treatment of **5** with *tert*-butyldimethylsilyl chloride in anhydrous THF, in the

Table 1. Physical Properties of 3-Amino-4-pyrazolecarbonitrile Derivatives **2a**−**m**

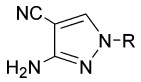

no.	R	yield (%)	recryst solv	mp (°C)	formula[a]
2a	$(CH_2)_5CH_3$	44	$CHCl_3$	119−120	$C_{10}H_{16}N_4$
2b	$(CH_2)_6CH_3$	52	CH_2Cl_2	96−97	$C_{11}H_{18}N_4$
2c	$(CH_2)_7CH_3$	54	*n*-hexane	84−85	$C_{12}H_{20}N_4$
2d	$(CH_2)_8CH_3$	56	*n*-heptane	88−89	$C_{13}H_{22}N_4$
2e	$(CH_2)_9CH_3$	49	cyclohexane	60−62[b]	$C_{14}H_{24}N_4$
2f	$(CH_2)_{10}CH_3$	41	cyclohexane	148−151	$C_{15}H_{26}N_4$
2g	$(CH_2)_{11}CH_3$	57	*i*-PrOH	108−111	$C_{16}H_{28}N_4$
2h	$CH_2C_6H_5$	70	AcOEt/cyclohexane	121−123[c]	$C_{11}H_{10}N_4$
2i	$CH_2CH_2C_6H_5$	80	AcOEt/cyclohexane	102−103[d]	$C_{12}H_{12}N_4$
2j	$CH_2CHOH(CH_2)_5CH_3$	70	EtOH	133−135	$C_{12}H_{20}N_4O$
2k	$CH_2CHOH(CH_2)_7CH_3$	50	EtOH	130	$C_{14}H_{24}N_4O$
(*R*)-**2k**	$CH_2CHOH(CH_2)_7CH_3$[e]	60	EtOH	124−126	$C_{14}H_{24}N_4O$
(*S*)-**2k**	$CH_2CHOH(CH_2)_7CH_3$[f]	41	EtOH	124−126	$C_{14}H_{24}N_4O$
2l	$CHCOCH_3(CH_2)_5CH_3$	88	cyclohexane	87−89	$C_{13}H_{20}N_4O$
2m	$CH(CHOHCH_3)(CH_2)_5CH_3$	45	*i*-PrOH	108−111	$C_{13}H_{22}N_4O$

[a] Elemental analyses for C, H, N were within ±0.4% of the calculated values. [b] Lett.[51] mp 69 °C. [c] Lett.[51] mp 132−134 °C. [d] Lett.[52] mp 98−100 °C. [e] $[\alpha]^{18}$ +120 (CH_3OH). [f] $[\alpha]^{18}$ −119 (CH_3OH).

Table 2. Physical Properties of Pyrazolo[3,4-*d*]pyrimidine Derivatives **3a**−**l**, **4**, and **8**

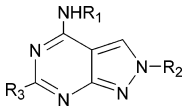

no.	R_1	R_2	R_3	yield (%)	recryst solv	mp (°C)	formula[a]
3a	H	$(CH_2)_5CH_3$	H	84	$CHCl_3$	215−217	$C_{11}H_{17}N_5$
3b	H	$(CH_2)_6CH_3$	H	32	AcOEt	205−208	$C_{12}H_{19}N_5$
3c	H	$(CH_2)_7CH_3$	H	38	AcOEt	208−210	$C_{13}H_{21}N_5$
3d	H	$(CH_2)_8CH_3$	H	26	AcOEt	200−202	$C_{14}H_{23}N_5$
3e	H	$(CH_2)_9CH_3$	H	25	AcOEt	196−198	$C_{15}H_{25}N_5$
3f	H	$(CH_2)_{10}CH_3$	H	30	AcOEt	192−195	$C_{16}H_{27}N_5$
3g	H	$(CH_2)_{11}CH_3$	H	44	AcOEt	168−170	$C_{17}H_{29}N_5$
3h	H	$CH_2C_6H_5$	H	75	AcOEt/cyclohexane	248−250	$C_{12}H_{11}N_5$
3i	H	$CH_2CH_2C_6H_5$	H	78	AcOEt/cyclohexane	188−190	$C_{13}H_{13}N_5$
3j	H	$CH_2CHOH(CH_2)_5CH_3$	H	70	*i*-PrOH	213-216	$C_{13}H_{21}N_5O$
3k	H	$CH_2CHOH(CH_2)_7CH_3$	H	64	EtOH	214−216	$C_{15}H_{25}N_5O$
(*R*)-**3k**	H	$CH_2CHOH(CH_2)_7CH_3$[b]	H	40	EtOH	206−208	$C_{15}H_{25}N_5O$
(*S*)-**3k**	H	$CH_2CHOH(CH_2)_7CH_3$[c]	H	34	EtOH	206−208	$C_{15}H_{25}N_5O$
3l	H	$CH(CHOHCH_3)(CH_2)_5CH_3$	H	45	EtOH	192−194	$C_{14}H_{23}N_5O$
4	$COCH_3$	$(CH_2)_9CH_3$	H	73	cyclohexane	90−92	$C_{17}H_{27}N_5O$
8	H	$(CH_2)_9CH_3$	C_6H_5	80	toluene	133	$C_{15}H_{16}N_4O$

[a] Elemental analyses for C, H, N were within ±0.4% of the calculated values. [b] $[\alpha]^{18}$ +51 (CH_3OH). [c] $[\alpha]^{18}$ −50 (CH_3OH).

Scheme 2

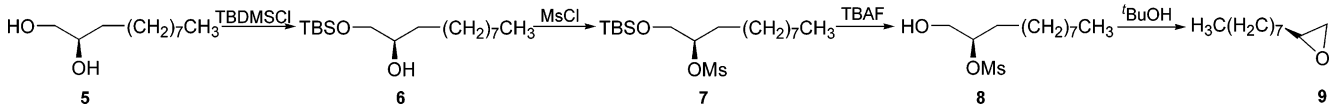

presence of imidazole, gave the C1-protected intermediate **6**, which was converted to mesylate **7** by reaction with methanesulfonyl chloride in anhydrous pyridine at 0 °C. Deprotection of **7** with tetrabutylammonium fluoride afforded the primary alcohol **8**, which provided the desired (*S*)-(−)-1,2-epoxydecane **9** by reaction with potassium *tert*-butoxide in MeOH.

The isomeric series of N^1-substituted pyrazolo[3,4-*d*]-pyrimidines **12a**−**i** were prepared as illustrated in Scheme 3. 4-Aminopyrazolo[3,4-*d*]pyrimidine **11** was obtained from **1** with boiling formamide, following a previously reported procedure.[25] The sodium salt of **11** was then alkylated with the suitable reactant in DMF solution at 100 °C to give the target inhibitors **12**. The appropriate alkyl bromide gave products **12a**−**e**, 1,2-epoxyoctane afforded the hydroxy derivative **12f**, and 3-bromononan-2-one[24] led to the keto derivative **12g**, which was converted to the desired **12h** by reduction with $NaBH_4$ in methanolic solution at room temperature. Ring closure of 5-amino-4-cyano-1-(β-hydroxyethyl)pyrazole **10**[26] with boiling formamide provided compound **12i**.

The synthetic route for compound **13** is shown in Scheme 4. A number of procedures have been described for the conversion of 3-amino-4-pyrazolecarbonitrile to 6-substituted pyrazolo[3,4-*d*]pyrimidines.[27,28] Since most of them require harsh conditions and proceed with poor yields, a new method for the synthesis of the candidate **13** was devised by us, which greatly reduced the reaction time and enhanced the yield of the product. This solventless method involved the mixing of 3-amino-1-decyl-4-pyrazolecarbonitrile **2e** and benzonitrile with

Scheme 3

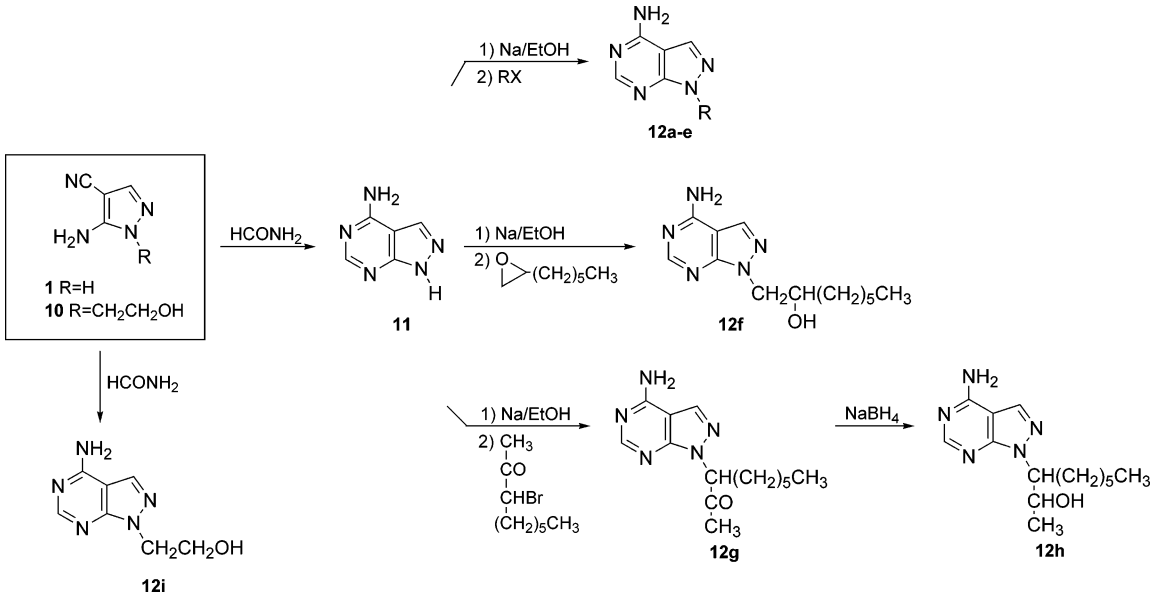

Table 3. Physical Properties of 4-Amino-1-alkylpyrazolo[3,4-*d*]pyrimidine Derivatives **7a**−**i**

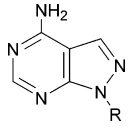

no.	R	yield (%)	recryst solv	mp (°C)	formula[a]
12a	$(CH_2)_9CH_3$	25	AcOEt	187−189	$C_{15}H_{25}N_5$
12b	$(CH_2)_{10}CH_3$	24	AcOEt	159−161	$C_{16}H_{27}N_5$
12c	$(CH_2)_{11}CH_3$	29	AcOEt	146−148	$C_{17}H_{29}N_5$
12d	$CH_2C_6H_5$	30	*i*-PrOH	238[b]	$C_{12}H_{11}N_5$
12e	$CH_2CH_2C_6H_5$	35	AcOEt	185	$C_{13}H_{13}N_5$
12f	$CH_2CHOH(CH_2)_5CH_3$	29	EtOH	146−148	$C_{13}H_{21}N_5O$
12g	$CH(COCH_3)(CH_2)_5CH_3$	40	−	oil	$C_{14}H_{21}N_5O$
12h	$CH(CHOHCH_3)(CH_2)_5CH_3$	60	−	oil	$C_{14}H_{23}N_5O$
12i	CH_2CH_2OH	96	toluene	217−219[c]	$C_7H_9N_5O$

[a] Elemental analyses for C, H, N were within ±0.4% of the calculated values. [b] Lett.[53] mp 235−236 °C. [c] Lett.[54] mp 223−224 °C.

Scheme 4

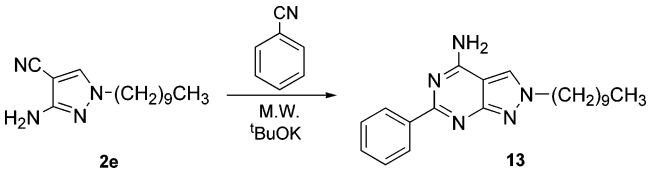

potassium *tert*-butoxide in an open glass tube, and irradiation of the reaction mixture in a household microwave oven for 3 min. The crude product was readily purified to afford the desired compound **13** with a high yield (80%).

Results and Discussion

Biological Evaluation. The K_i values for inhibition of bovine spleen ADA by aminopyrazolopyrimidine derivatives **3a**−**l**, **4**, **12a**−**f**,**h**,**i**, and **13** are presented in Table 4. (+)-EHNA was used as the reference standard.

Results showed that the 2-substituted aminopyrazolopyrimidine derivatives **3** were in general more potent than their 1-substituted analogues **12**, with compounds **3d**−**f**,**j**,**k** exhibiting K_i values in the nanomolar/subnanomolar range. It should be noted that the inhibitory activity in the 2-substituted aminopyrazolopyrimidine series is enhanced with the increasing of the length of the side alkyl chain (**3a** < **3b** < **3c** < **3d** < **3e** ≈ **3f**), reaching its maximum with the *n*-decyl and the *n*-undecyl chains of **3e** and **3f** showing K_i values of 0.13 nM and 0.47 nM, respectively, 1 order of magnitude lower than that of (+)-EHNA (1.14 nM). Further increase in the length of the side chain was dramatically detrimental for activity (compound **3g**, K_i > 10000 nM).

Insertion of a 2′-hydroxy group into the *n*-octyl chain of **3c** (K_i 530 nM) led to compound **3j** whose inhibitory activity was 3 orders of magnitude higher than that of the parent compound. The remarkable beneficial effect of the 2′-hydroxy group in **3j** may be related to the formation of an additional H-bond with the enzyme.

The β-hydroxy substitution on the *n*-decyl chain of the potent inhibitor **3e** gave compound **3k**, which proved to be highly potent, like its parent derivative (K_i 0.28 nM). As it is well-known that the ADA inhibitory potency of EHNA depends on the stereochemistry of its side chain, the two enantiomers of **3k** were prepared and tested. The (*R*)-**3k** isomer (K_i 0.053 nM) proved to be the most active compound of the whole series, more

Table 4. ADA Inhibition Data of Derivatives **3a**−**l**, **4**, **12a**−**f**,**h**,**i**, and **13**

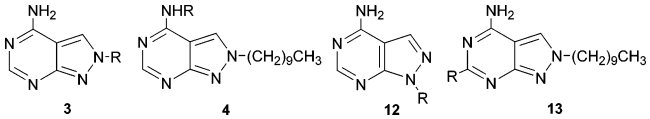

no.	R	K_i (nM)[a]
3a	$(CH_2)_5CH_3$	n.a.[b]
3b	$(CH_2)_6CH_3$	818 ± 62.3
3c	$(CH_2)_7CH_3$	530 ± 44.5
3d	$(CH_2)_8CH_3$	8.05 ± 0.20
3e[c]	$(CH_2)_9CH_3$	0.13 ± 0.01
3f[c]	$(CH_2)_{10}CH_3$	0.47 ± 0.02
3g	$(CH_2)_{11}CH_3$	n.a.
3h	$CH_2C_6H_5$	n.a.
3i	$CH_2CH_2C_6H_5$	n.a.
3j[c]	$CH_2CHOH(CH_2)_5CH_3$	1.00 ± 0.08
3k[c]	$CH_2CHOH(CH_2)_7CH_3$	0.28 ± 0.02
(*R*)-**3k**[c]	$CH_2CHOH(CH_2)_7CH_3$	0.053 ± 0.003
(*S*)-**3k**	$CH_2CHOH(CH_2)_7CH_3$	37.5 ± 3.36
3l	$CH(CHOHCH_3)(CH_2)_5CH_3$	53.4 ± 4.82
4	$COCH_3$	n.a.
12a	$(CH_2)_9CH_3$	n.a.
12b	$(CH_2)_{10}CH_3$	n.a.
12c	$(CH_2)_{11}CH_3$	n.a.
12d	$CH_2C_6H_5$	n.a.
12e	$CH_2CH_2C_6H_5$	n.a.
12f	$CH_2CHOH(CH_2)_5CH_3$	n.a.
12h	$CH(CHOHCH_3)(CH_2)_5CH_3$	66.1 ± 4.31
12i	CH_2CH_2OH	4619 ± 386
13	C_6H_5	n.a.
(+)-EHNA		1.14 ± 0.10

[a] The K_i values are means ±SEM. [b] n.a.: non active. Inhibition occurred at a concentration higher than 10^{-5} M. [c] This compound displayed no significant affinity at bA_1, bA_{2A}, and bA_3ARs.

potent than the (*S*)-**3k** isomer (K_i 37.5 nM) and the parent compound **3e** (K_i 0.13 nM). (*R*)-**3k** therefore presents the best spatial relationship among the pharmacophoric groups, adequately fulfilling the stereoselectivity of the ADA binding site. Only a modest result was obtained when the EHNA 9-(2-hydroxy-3-nonyl) side chain was inserted at position 2 of the aminopyrazolopyrimidine system, seeing that compound **3l** showed a K_i in the submicromolar range. Substitution of the *n*-alkyl chains with arylalkyl groups, as in compounds **3h**,**i**, is totally detrimental for ADA inhibitory activity.

In agreement with the findings of Schaeffer[22] for EHNA derivatives, also in the aminopyrazolopyrimidine series the insertion of a substituent on the N^4 of the very active compound **3e** led to a complete loss of activity (compound **4**, $K_i > 10000$ nM). Surprisingly, also the 6-phenyl derivative of **3e**, compound **13**, was completely inactive, in contrast with findings reported in the literature[21] for a similar substitution on EHNA.

The shift of the substituents from position 2 to position 1 of the aminopyrazolopyrimidine system, to give compounds **12a**−**f**,**h**,**i**, was detrimental to the ADA inhibitory activity. None of the 1-substituted aminopyrazolopyrimidines showed any inhibitory potency, the only exception being compound **12h**, bearing the EHNA side chain, which was equipotent with its 2-substituted counterpart **3l**. The insertion at position 1 of a small hydroxyalkyl group, as in compound **12i**, did not give any appreciable results, either.

The binding affinities of the most potent aminopyrazolopyrimidine derivatives **3e**, **3f**, **3j**, **3k**, and (*R*)-**3k** at the bovine A_1, A_{2A}, and A_3ARs were also determined. All the aminopyrazolopyrimidines were fully selective for ADA, since none of them displayed any significant affinity at the A_1, A_{2A}, or A_3ARs (data not shown). The newly synthesized aminopyrazolopyrimidine derivatives thus appear to be an interesting class of potent, fully selective ADA inhibitors.

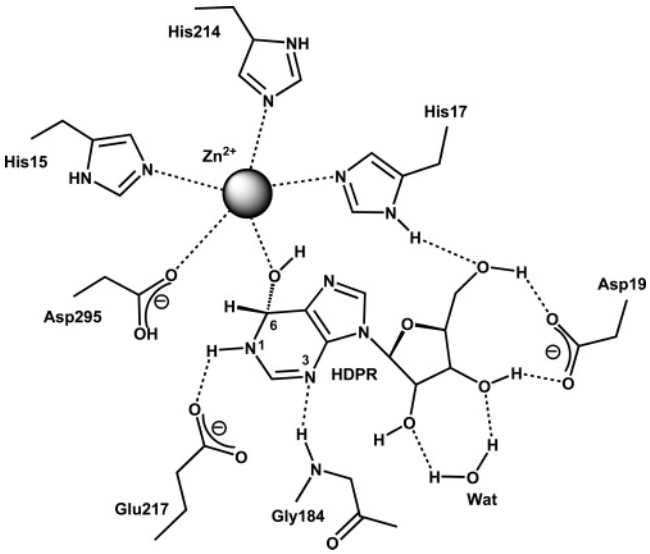

Figure 1. Schematic representation of important protein−ligand interactions in the reported[29] crystal structure of the ADA−HDPR complex.

Molecular Modeling. In literature, no data are reported about the crystal structure of ADA complexed with a semi-tight-binding inhibitor such as EHNA. Only the structure of murine ADA complexed with HDPR, an almost ideal transition-state analogue, is available, and this led to the following discoveries concerning the catalytic activity of the enzyme: (i) a Zn^{2+} cofactor is bound into the active site located in a deep pocket at the C-terminus of the β-barrel; (ii) the localization of the zinc and key catalytic residues confer the precise stereospecificity of the site and of the hydrolytic reaction; (iii) the active site with bound HDPR is buried and made inaccessible to the bulk solvent by a hinged motion of one or two peptide loops that serve as lids to the active site pocket; (iv) the Zn^{2+} is coordinated by the ϵ nitrogens ($N^{\epsilon 2}$) of His15, His17, and His214, by a carboxylate oxygen ($O^{\delta 2}$) of Asp295, and by the hydroxyl oxygen (6-OH) of the HDPR inhibitor, as schematically shown in Figure 1.

To better understand the high ADA inhibitory potency of compounds **3e** and **3k** at a molecular level, docking experiments were performed on the binding pocket of the murine ADA/HDPR complex.[29] The most active 2′*S*,3′*R*-*erythro*-enantiomer of EHNA, (+)-EHNA, was also docked into the catalytic site of the enzyme for a proper comparison, which might have helped us to better delineate the SARs of our compounds. For less active or inactive compounds, docking was carried out in an attempt to elucidate the reasons behind the reduced biological activity. Docking experiments were carried out using the automated docking program AutoDock,[30] which allows torsional flexibility in the ligand and incorporates an efficient Lamarckian genetic search algorithm, together with an empirical free energy function. With recent improvements in search algo-

Table 5. Results of 50 Independent Docking Runs for Each Ligand[a]

ligand	N_{tot}	f_{occ}	ΔG_{bind}	surrounding residues
(+)-EHNA	15	20	−10.4	His15, **His17**, Asp19, Gly20, Phe61, Leu62, Phe65, Asp66, Arg101, Tyr102, Ser103, Leu106, Trp117, **Cys153**, Cys154, Met155, Arg156, His157, Asp181, Leu182, Ala183, Gly184, Asp185, His214, Glu217, His238, Ser265, **Asp295**, **Asp296**, Phe300
3e	15	4	−10.3	His15, His17, Asp19, Gly20, Leu58, Phe61, Leu62, Ala63, Phe65, Asp66, Met69, Tyr102, Ser103, Leu106, Trp117, Cys153, Met155, His157, Trp161, Ala183, **Gly184**, Asp185, Glu186, His214, Glu217, His238, Ser265, Thr269, **Asp295**, **Asp296**, Phe300
(*R*)-**3k**	31	21	−10.8	His15, **His17**, Leu18, Asp19, Gly20, Leu58, Phe61, Leu62, Ala63, Phe65, Asp66, Met69, Arg101, Tyr102, Ser103, Leu106, Trp117, Cys153, Met155, His157, Ala183, **Gly184**, Asp185, Glu186, His214, Glu217, His238, Ser265, Thr269, **Asp295**, **Asp296**, Phe300

[a] N_{tot} is the total number of clusters; the number of results in the top cluster is given by the frequency of occurrence, f_{occ}; ΔG_{bind} is the estimated free energy of binding for the top cluster results and is given in kcal/mol. The last column shows the contacting residues for the binding mode of the top cluster. Only residues with at least 5 Å van der Waals contacts to the ligand are shown. Residues that form hydrogen bonds with the ligand are highlighted in bold. Zinc coordinating residues are underlined.

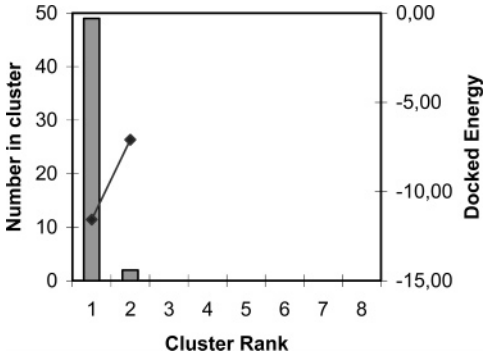

Figure 2. AutoDock results for docking of HDPR into the ADA crystal structure.

rithms and energy functions, computational docking methods have become a valuable tool to probe the interaction between an enzyme and its inhibitors in the absence of detailed experimental data and can contribute significantly to the understanding of its structural and energetic basis.[31]

Although the inhibition assays on our compounds were conducted on bovine ADA, the use of the crystal structure of murine ADA for docking studies is justified by the following facts: (i) the bovine and mouse sequences of this enzyme are characterized by 85% of homology; (ii) all active-site residues are largely preserved across the ADA isoforms so far sequenced; (iii) the bovine and mouse ADA complexed with HDPR have similar conformations and are particularly similar around the active site, suggesting that the two enzyme species might be functionally interchangeable.[32]

Prior to automated docking of the reported inhibitors, HDPR itself was docked into the ADA crystal structure as a means of testing program performance. The docking test indicated that the largest cluster of similar conformations with the lowest energy docked structure reproduced very closely the crystallographic binding mode of HDPR to ADA (Figure 2). The hydrogen bonds predicted by AutoDock were virtually identical to those found in the crystal structure.

Docking of (+)-EHNA, **3e** and both (*R*)- and (*S*)-isomers of **3k** revealed a consistent set of recurring binding modes. For the three ligands investigated, well-clustered docking results were obtained. As shown in Table 5, the 50 independent docking runs carried out for each ligand generally converged to a higher-than-average number of different positions ("clusters" of results differing by less than 1.5 Å rmsd). Such a higher-than-average number of clusters is due to the fact that these compounds are large and highly flexible, but nevertheless most of the results are found in the top two clusters. Generally, the top clusters (i.e. those with the most favorable ΔG_{bind}) were also associated with the highest frequency of occurrence, which suggests a good convergence behavior of the search algorithm. As regards the estimated free energies of binding, they compare well with experimental inhibition constants, correctly suggesting affinities in the subnanomolar range. The best results in terms of free energy of binding were all located in a similar position at the active site. The most important interactions found for each compounds are summarized in Table 5.

Docking of (+)-EHNA to the ADA crystal structure revealed a very clear preference for a single position in the active site. The corresponding result was ranked with the best binding energy (estimated $\Delta G_{bind} = -10.4$ kcal/mol) and was found 20 times in 50 independent docking runs. The ligand was found to be in the same location as HDPR in the crystal structure. As illustrated in Figure 3a, the adenine NH_2 group formed hydrogen bonds with the Asp295 $O^{\delta 1}$ oxygen and the Asp296 $O^{\delta 1}$ and $O^{\delta 2}$ oxygens. The 2′-hydroxy group was involved in hydrogen bonds with the $N^{\delta 1}$ hydrogen of His17 and the S^{γ} hydrogen of Cys153. A small hydrophobic pocket, framed by the residues Met55, Ala183, and Gly184, was found to accommodate the 1′-methyl group. The hydrophobic alkyl chain was located at the entrance of the enzyme binding pocket, where it formed numerous favorable lipophilic interactions. These results are in agreement with the SAR studies, which suggest distinct binding pockets for the 1′-methyl and 2′-hydroxy groups and the hydrophobic alkyl chain.[33] Moreover, inspection of the binding position of (+)-EHNA at the active site revealed that no hydrogen bond was formed between the main chain NH of Gly184 and the N3 nitrogen of the ligand.

In the most frequently occurring and most favorable result (−11.3 kcal/mol, found 27 times out of 50), compound **3e** was found to bind in the known binding pocket, in a manner similar to that of HDPR and (+)-EHNA, with the long lipophilic chain localized in a deep and narrow channel at the entrance of the enzyme (Figure 3b). In addition, one of the 4-NH_2 hydrogens was involved in a hydrogen bond with the $O^{\delta 2}$ atom of Asp296, while the other hydrogen formed a hydrogen bond with the $O^{\delta 1}$ atom of Asp295. Moreover, the N7

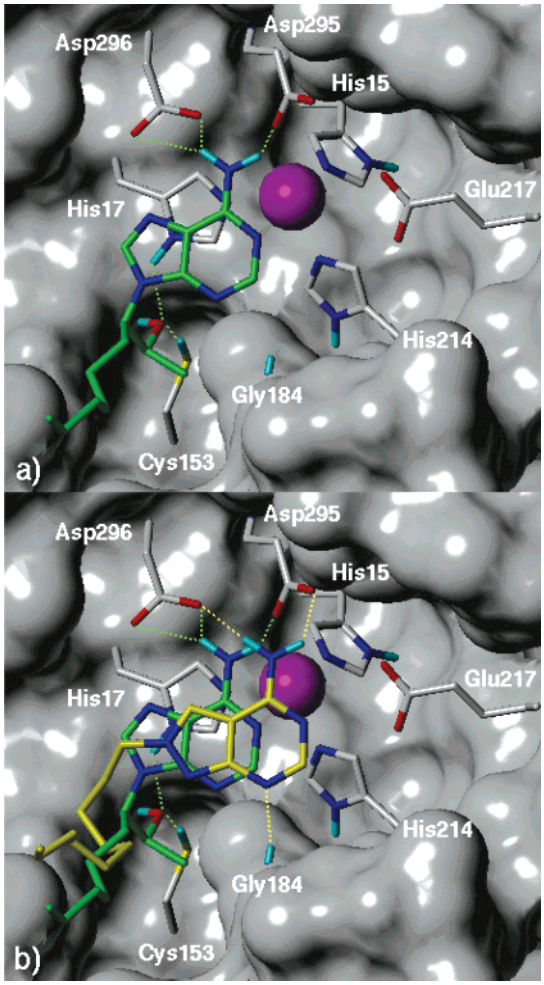

Figure 3. (a) Docked structure of (+)-EHNA (green) in the ADA active site displayed as a Connolly surface. (b) Superimposition of (+)-EHNA (green) and compound **3e** (yellow) bound to the ADA binding pocket. The residues involved in hydrogen bonding to ligands are also indicated, with their residue type and sequence numbers written in white. The zinc ion is shown in magenta. Hydrogen bonds are represented with dashed lines. Nonpolar hydrogens were removed for clarity.

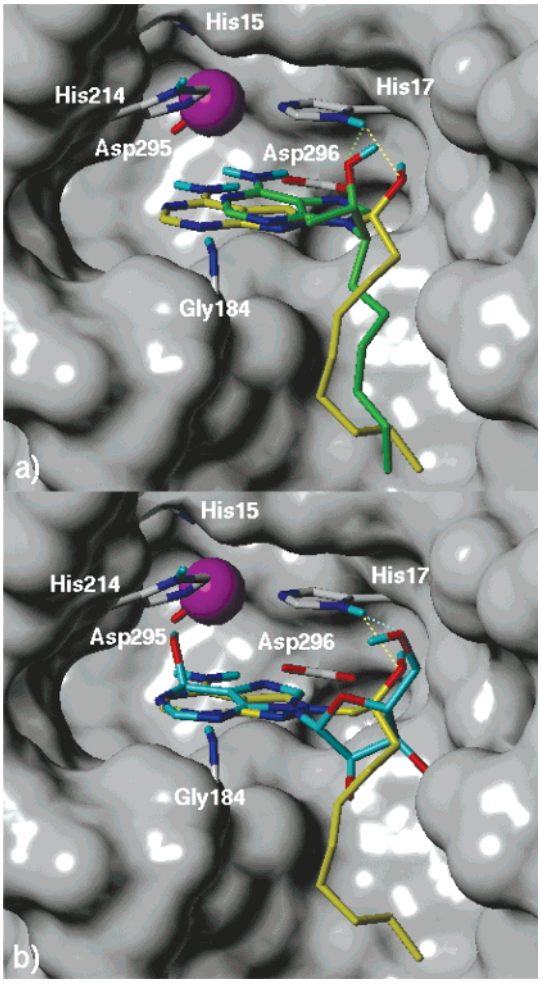

Figure 4. Comparison of ligand-binding modes revealed by docking: (a) superposition of the (*R*)-enantiomer of **3k** (yellow) and (+)-EHNA (green); (b) superposition of the (*R*)-enantiomer of **3k** (yellow) and HDPR[29] (cyan). The enzyme active site is displayed as a Connolly surface.

nitrogen of the pyrazolopyrimidine system accepted a hydrogen bond from the main chain nitrogen of Gly184.

As shown in Figure 3b, the binding of **3e** to ADA is very similar to that observed for (+)-EHNA binding. All hydrogen bonds between ADA and (+)-EHNA are retained in the ADA/**3e** complex, with a further hydrogen bond being formed between the N7 of **3e** and the backbone NH of Gly184, which is not possible for the N3 of (+)-EHNA. Actually, the superimposed structures show that the purine ring of (+)-EHNA is slightly displaced from the position of **3e**, away from Gly184. This is consistent with the SAR data showing that **3e** is 9-fold more potent than (+)-EHNA in the ADA inhibitory assay, with a K_i of 0.13 nM.

As **3k** is a chiral compound, both enantiomers were considered for docking. For the (*R*)-enantiomer, only one distinct binding position in the active site was obtained: the result with the top binding energy (−10.8 kcal/mol) was found 21 times out of 50. The structure of the ligand revealed a binding mode very similar to those previously described for **3e** into ADA. In addition, a further hydrogen bond was observed between the 2-hydroxy group of the inhibitor and the $N^{\delta 1}$ of His17, making a significant contribution to the inhibitor binding stabilization, consistent with the 2.5-fold higher potency displayed by (*R*)-**3k** (K_i 0.053 nM) with respect to **3e** (K_i 0.13 nM). As illustrated in Figure 4, superimposition of the enzyme-bound conformation of (*R*)-**3k** on that of (+)-EHNA (Figure 4a) and HDPR (Figure 4b) suggests that the 2-hydroxy group of (*R*)-**3k**, the 2′-hydroxy group of (+)-EHNA, and the 5′-hydroxy group of HDPR point to the same hydrogen bond donor, His17.

In the case of the (*S*)-enantiomer of **3k**, the automated docking calculations did not converge to a highly populated cluster. In fact, inspection of the docked structures revealed that many of the top-ranked clusters did not fit properly into the active site, as the pyrazolopyrimidine system pointed outside the enzyme cleft. It should be noted that this (*S*)-enantiomer showed a K_i value (37.5 nM) 4 orders of magnitude higher than that of the other stereoisomer.

In an effort to elucidate the reasons for the inactivity of aminopyrazolopyrimidine derivatives bearing the alkyl chain in position 1 (**12a**−**i**), the docking of compound **12a** was carried out. The molecule occupied the same space as **3e**, with the 4-NH_2 involved in hydrogen bonds with the Asp295 $O^{\delta 2}$ and Glu217 $O^{\epsilon 2}$ oxygens, and the long lipophilic chain located at the entrance position of the enzyme. However, **12a** appeared to be signifi-

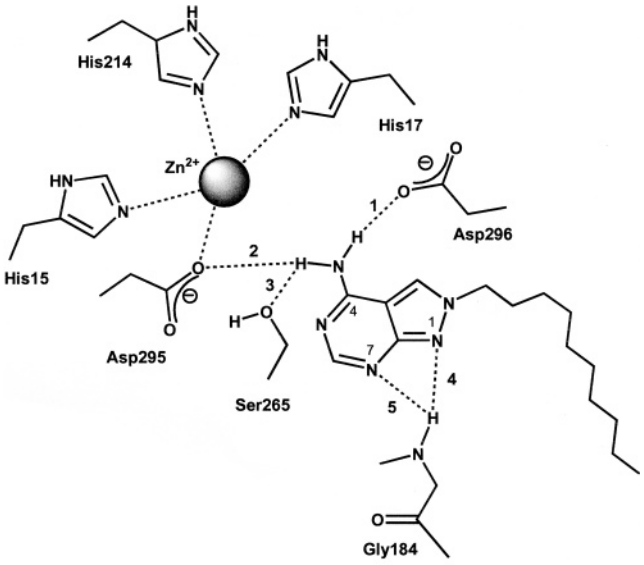

	Interatomic Distance (Å)	
1	[HN ···· O]	2.4±0.7
2	[HN ···· O]	2.8±0.6
3	[HN ···· O]	3.4±0.3
4	[N ···· HN]	2.7±0.3
5	[N ···· HN]	2.5±0.3

Figure 5. Schematic representation of the main interactions observed in the molecular dynamics simulation of compound **3e** bound to ADA. Mean values of intermolecular hydrogen bond distances and of their standard deviations are given.

cantly displaced from the binding position of inhibitor **3e**. As a result of this displacement, the 4-NH_2 nitrogen was too far away for significant hydrogen bond formation with the catalytic residue Asp296. Moreover, the binding mode of the ligand did not allow the formation of the hydrogen bond between the N7 nitrogen of the pyrazolopyrimidine system and the Gly184 NH backbone. Thus, the drastic reduction of the ADA inhibitory activity of **12a**−**i** might be ascribed to the shifting in the position of the ligand in the active site, which does not allow the formation of hydrogen bonds with the essential catalytic residues Asp296 and Gly184.

To assess the dynamic stability of the ADA/**3e** complex, and to analyze the potential ligand−receptor interactions, a molecular dynamics (MD) simulation in a solvated system was run at room temperature. The main features of the final docking model are schematically represented in Figure 5, together with the interatomic distances for all important polar interactions. The three-dimensional structure of the ADA/**3e** complex is shown in Figure 6.

The root-mean-square (rms) deviation of the zinc and its coordinating ligands (His15, His17, His214, and Asp295) was calculated with respect to the crystal structure at various times during the simulation. In each case, the rms deviation was <0.6 Å, which indicates that the model of the zinc and its ligands retains the trigonal bipyramid geometry observed in the crystal structure with the $N^{\epsilon 2}$ atoms of His15 and His17 occupying the vertexes of the triangle, and His214 $N^{\epsilon 2}$ and Asp295 $O^{\delta 2}$ occupying the apexes.

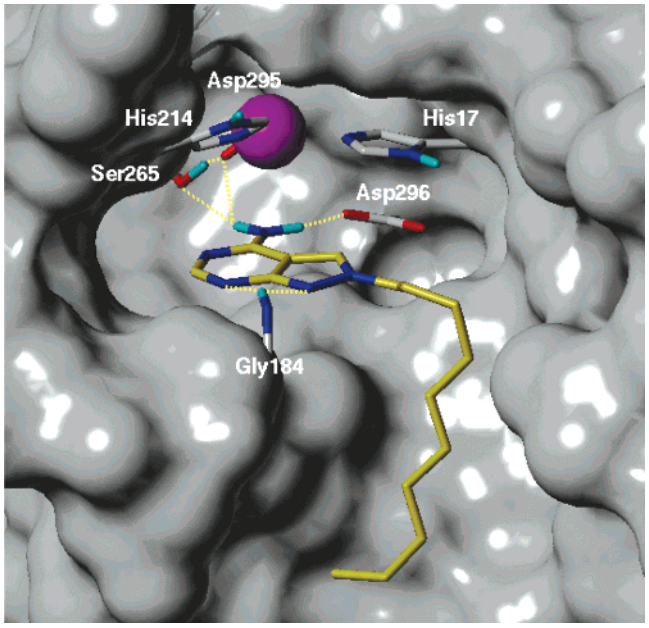

Figure 6. Docked structure of inhibitor **3e** (yellow) in the ADA active site, displayed as a Connolly surface, after 200 ps of MD simulations.

One of the amino hydrogen atoms formed a stable hydrogen bond with the $O^{\delta 2}$ atom of Asp296 (bond 1). The other hydrogen atom of the amino group also appeared to be involved in two hydrogen bonds with the $O^{\delta 1}$ atom of Asp295 (bond 2) and the O^{γ} of Ser265 (bond 3), although this latter bond was observed to be frequently cleaved in the simulation, giving an average distance longer than that of an ideal hydrogen bond. This result is in agreement with the SAR data, indicating that the 4-NH_2 is the primary determinant for binding of our inhibitors. In fact, substitution at the N^4 position of **3e** with the acetyl substituent leads to compound **4**, whose inactivity is due to a steric hindrance and to a change in the optimal binding mode of the ligand. Two hydrogen bonds between the N1 and N7 atoms of the inhibitor pyrazolopyrimidine system (bonds 4 and 5) and the main chain nitrogen of Gly184 were also shown to contribute to the complex stabilization.

The pyrazolopyrimidine nucleus of the inhibitor **3e** is located in a hydrophobic pocket defined by Thr269, Leu58, Phe61, Phe300, Leu62, and Phe65 side chains, which contribute to the formation of the floor of the cavity. The long hydrophobic alkyl chain fits snugly into a narrow, deep, and highly hydrophobic cleft which reaches the active-site entrance and consequently makes extensive hydrophobic contact with the residues Leu62, Ala63, Phe65, Ala183, and Gly184 on one side and Met69, Leu106, Trp117, and Met155 on the opposite side. Thus, the length of the *n*-alkyl substituent in the aminopyrazolopyrimidine series is the critical attribute for potent inhibitors. It is important to mention that the binding site model proposed here suggests that the optimal alkyl chain length ranges between 10 and 11 carbons. The loss of inibitory activity of compound **3g**, which differs from **3e** in the presence of a longer alkyl chain, might be due to an unfavorable interaction of the emerging chain with the solvent at the end of the channel or, more probably, to the inability of **3g** to enter

into the binding pocket, due to an unsuitable hydrophilic/hydrophobic balance affecting the properties of the ligand.

The shape of the *n*-alkyl substituent is also important for the ligand interactions. As shown in Table 4, structural changes which alter the shape of the *n*-alkyl substituent lead to significant changes in its inhibitory activities. Manual superposition of compounds **3h** and **3i** on the docked structure of **3e** reveals a steric repulsion between the phenyl ring of these compounds and the walls of the hydrophobic cleft, thus explaining their detrimental effect on the ADA inhibitory activity. In the case of the inactive compound **13**, the automated docking calculations did not converge toward a single binding position. From a visual inspection of the ADA/**13** complex, it seems clear that the presence of a phenyl ring in the 6 position of the pyrazolopyrimidine system increases the steric hindrance inside the binding cavity and changes the optimal binding mode of the ligand, decreasing the relative stability of the complex.

The docking simulation performed on the aminopyrazolopyrimidine compounds into the ADA binding site helped to rationalize the SARs of these inhibitors and to highlight the key pharmacophoric elements that make it possible to interact optimally with the enzyme, thus prospectively guiding the design of new analogues.

Experimental Section

1. Chemistry. Melting points were determined using a Reichert Köfler hot-stage apparatus and are uncorrected. IR spectra were recorded with a Pye Unicam Infracord Model PU956 in Nujol mulls. Routine ^{1}H NMR spectra were determined on a Varian Gemini 200 spectrometer using DMSO-d_6 as the solvent. Specific rotation of optically active compounds was measured on an Optically Activity LTD polarimeter at the sodium D light. Evaporation was performed in vacuo (rotary evaporator). Anhydrous sodium sulfate was always used as the drying agent. Analytical TLC was carried out on Merck 0.2 mm precoated silica gel (60 F-254) aluminum sheets, with visualization by irradiation with a UV lamp. Flash chromatography was performed with Merck Silica gel 60 (230−400 mesh ASTM). Elemental analyses were performed by our Analytical Laboratory and agreed with theoretical values to within ±0.4%. The microwave-assisted procedure was carried out in a household microwave (MW) oven equipped with a turntable and operating at 2.450 MHz. An alumina bath (Merck Aluminum oxide 90, 70−230 mesh ASTM) was used as a heat sink inside the MW oven to irradiate the reaction mixture. The average temperature at the end of the reaction was measured by inserting a thermometer in the alumina bath housing the reaction vessel.

The alkyl bromides used to obtain compounds **2a**−**i** and **12a**−**e**, 3-amino-4-pyrazolecarbonitrile, 1,2-epoxyoctane, 1,2-epoxydecane, (*R*)-(+)-1,2-epoxydecane, (*R*)-(+)-1,2-decanediole, and 2-nonanone were from Sigma-Aldrich. All other chemicals were of reagent grade.

The following products were prepared in accordance with literature procedures: 3-bromononan-2-one;[24] 4-aminopyrazolo-[3,4-*d*]pyrimidine **11**,[25] 5-amino-1-(β-hydroxyethyl)-4-pyrazolecarbonitrile **10**.[26]

General Procedure for the Synthesis of 1-Alkyl-3-amino-4-pyrazolecarbonitriles 2a−**i.** The appropriate alkyl bromide (12 mmol) was added dropwise to a suspension of 3-amino-4-pyrazolecarbonitrile **1** (1.08 g, 10 mmol) and anhydrous potassium carbonate (1.66 g, 12 mmol) in 10 mL of DMF. The reaction mixture was stirred at 100 °C until the disappearance of the starting material (2−8 h, TLC analysis). After cooling, the inorganic material was filtered off and the solution was evaporated to dryness under reduced pressure. The residue was then purified by flash chromatography (eluting system: ethyl acetate/petroleum ether 60−80 °C 7/3) to obtain **2a**−**i** as a white solid, which was recrystallized from the appropriate solvent (Table 1).

General Procedure for the Synthesis of 3-Amino-1-β-hydroxyalkyl-4-pyrazolecarbonitriles 2j,k,(*R*)-2k,(*S*)-2k. The appropriate 1,2-epoxyalkane (12 mmol) was added dropwise to a suspension of 3-amino-4-pyrazolecarbonitrile **1** (1.08 g, 10 mmol) and anhydrous potassium carbonate (1.66 g, 12 mmol) in 10 mL of DMF. The reaction mixture was stirred at 100 °C until the disappearance of the starting material (1−4 h, TLC analysis). After cooling, the salt was filtered off and the solution was evaporated to dryness under reduced pressure. The residue was then recrystallized from the appropriate solvent to obtain the target compounds **2j**,**k** (Table 1).

3-Amino-1-(2-keto-3-nonyl)-4-pyrazolecarbonitrile 2l. A suspension of 3-amino-4-pyrazolecarbonitrile **1** (1.08 g, 10 mmol), 3-bromononan-2-one[24] (2.65 g, 12 mmol), and anhydrous potassium carbonate (1.66 g, 12 mmol) in 10 mL of DMF was heated under stirring at 100 °C for 2 h. After cooling, the inorganic material was filtered off and the solution was evaporated to dryness under reduced pressure. The residue was then purified by flash chromatography (eluting system: ethyl acetate/cyclohexane 3/7) to obtain **2l** as a pale yellow solid, which was purified by recrystallization and characterized as a racemic mixture (Table 1).

3-Amino-1-(2-hydroxy-3-nonyl)-4-pyrazolecarbonitrile 2m. $NaBH_4$ (1.13 g, 30 mmol) was added portionwise to an ice-cooled solution of **2l** (2.48 g, 10 mmol) in 30 mL of methanol, while maintaining the pH between 5 and 6 by adding glacial acetic acid. Once addition was complete, stirring was continued at room temperature for 22 h. The reaction mixture was then concentrated in vacuo and the residue was neutralized with saturated $NaHCO_3$ solution and extracted with chloroform. The combined organic extracts were dried, filtered, and evaporated to dryness under reduced pressure. The resulting crude product was purified by flash chromatography (eluting system: ethyl acetate/cyclohexane 5/5) to obtain the target compound **2m** as a pure yellow oily product, which was characterized as a diastereomeric mixture (Table 1).

General Procedure for the Synthesis of 2-Alkyl-4-aminopyrazolo[3,4-*d*]pyrimidines 3a−**l.** A suspension of 1-alkyl-3-amino-4-pyrazolecarbonitrile **2a**−**k**,**m** (10 mmol) in 3 mL of formamide was vigorously boiled, under stirring, until the disappearance of the starting material (4−16 h, TLC analysis). The cooled solution was then diluted with ice−water, and the solid separated was filtered, washed with water, and recrystallized from the appropriate solvent (Table 2).

4-Acetylamino-2-decylpyrazolo[3,4-*d*]pyrimidine 4. A suspension of 4-amino-2-decylpyrazolo[3,4-*d*]pyrimidine **3e** (2.27 g, 10 mmol) and acetic anhydride (1.41 mL, 15 mmol) in 10 mL of pyridine was heated at 100 °C under stirring for 2 h. The volatiles were then removed in vacuo, and the residue was diluted with ice−water. The resulting solid was collected and recrystallized from cyclohexane to give the target compound **4** as a pale yellow crystalline solid (Table 2).

1-(*tert*-Butyldimethylsilanyloxy)-decan-2-ol 6. *tert*-Butyldimethylsilyl chloride (TBDMSCl, 1.51 g, 10 mmol) was added under nitrogen to an ice-cooled solution of (*R*)-(+)-1,2-decanediole **5** (1.74 g, 10 mmol; $[\alpha]^{23}$ +12, c = 0.5, CH_3OH) in anhydrous THF containing imidazole (0.680 g, 20 mmol). The reaction mixture was stirred at room temperature for 18 h, then diluted with Et_2O and washed sequentially with water and brine. The organic layer was dried, filtered, and evaporated to dryness under reduced pressure. The residue was purified by flash chromatography (eluting system: ethyl acetate) to obtain the target compound **6** as a pure oily product with a 72% yield. $[\alpha]^{18}$ +13.2 (CH_3OH). IR, ν cm^{-1}: 3395, 1102, 830. ^{1}H NMR, δ ppm: 0.018 (s, 6H, $SiCH_3$), 0.85 (s, 12H, CH_3), 1.23 (bs, 12H, CH_2), 1.36 (bs, 2H, CH_2), 3.15−3.23 (m, 3H, $CHCH_2$), 4.34 (dd, 1H, OH, exc). Anal. ($C_{16}H_{36}O_2Si$) C, H.

1-(*tert*-Butyldimethylsilanyloxymethyl)nonyl Methanesulfonate 7. Methanesulfonyl chloride (MsCl, 0.93 mL, 12 mmol) was added dropwise to an ice-cooled solution of the

alcohol **6** (2.88 g, 10 mmol) in anhydrous pyridine. The reaction mixture was stirred at room temperature for 12h, then diluted with Et_2O and washed with water. The organic layer was dried, filtered, and evaporated to dryness under reduced pressure. The residue was purified by flash chromatography (eluting system: ethyl acetate) to afford mesylate **7** as a pure oily product with a 52% yield. $[\alpha]^{18}$ +40 (CH_3OH). IR, ν cm^{-1}: 3411, 1250, 1168, 1050. ^1H NMR, δ ppm: 0.053 (s, 6H, $SiCH_3$), 0.84 (s, 12H, CH_3), 1.24 (bs, 12H, CH_2), 1.63 (bs, 2H, CH_2), 3.14 (s, 3H, CH_3), 3.23 (d, 2H, CH_2). Anal. ($C_{17}H_{38}O_4SSi$) C, H.

1-(Hydroxymethyl)nonyl Methanesulfonate 8. An ice-cooled solution of the mesylate **7** (3.66 g, 10 mmol) in anhydrous THF was treated dropwise with tetrabutylammonium fluoride 1.0 M solution in THF (10 mL, 10 mmol). The reaction mixture was stirred at room temperature for 18 h, then diluted with water and extracted with Et_2O. The combined organic extracts were dried, filtered, and evaporated to dryness under reduced pressure. The resulting oily product was purified by flash chromatography (eluting system: ethyl acetate) to obtain the target compound **8** as a pure pale yellow oil with a 76% yield. $[\alpha]^{18}$ +45 (CH_3OH). IR, ν cm^{-1}: 3539, 1260, 1168. ^1H NMR, δ ppm: 0.86 (t, 3H, CH_3), 1.24 (bs, 12H, CH_2), 1.60 (m, 2H, CH_2), 3.22 (d, 1H, CH_2), 3.14 (s, 3H, CH_3), 3.52 (dd, 1H, CH), 5.07 (t, 1H, OH, exc). Anal. ($C_{11}H_{24}O_4S$) C, H.

(*S*)-(−)-Epoxydecane 9. A solution of the alcohol **8** (2.52, 10 mmol) and potassium *tert*-butoxide (1.12 g, 10 mmol) in MeOH was stirred at room temperature for 8 h, then partitioned between CH_2Cl_2 and water. The aqueous layer was further extracted with CH_2Cl_2, and the combined organic phases were dried, filtered, and evaporated to dryness under reduced pressure. The resulting oily product was purified by flash chromatography (eluting system: ethyl acetate) to obtain the target compound **9** as a pure oil with an 80% yield. $[\alpha]^{18}$ −14.0 (c = 1.0, Et_2O) (Lett.[34] $[\alpha]_D$ −14.7, c = 1.44, Et_2O). IR, ν cm^{-1}: 1460, 1367. ^1H NMR, δ ppm: 0.85 (t, 3H, CH_3), 1.24 (bs, 12H, CH_2), 1.41 (m, 2H, CH_2), 2.41 (dd, 2H, CH_2), 2.85 (m, 1H, CH). Anal. ($C_{10}H_{20}O$) C, H.

General Procedure for the Synthesis of 1-Alkyl-4-aminopyrazolo[3,4-*d*]pyrimidines 12a−e. 4-Aminopyrazolo[3,4-*d*]pyrimidine[25] **11** (1.35 g, 10 mmol) was added under a nitrogen atmosphere to a solution of sodium (0.276 g, 12 mmol) in 25 mL of absolute ethanol. The solvent was then removed in vacuo, and the resulting sodium salt was suspended in DMF. The appropriate alkyl bromide (12 mmol) was added dropwise, and the reaction mixture was stirred at 100 °C until the disappearance of the starting material (1−3 h, TLC analysis). After cooling, the reaction mixture was concentrated in vacuo and the residue was diluted with ice−water. The resulting solid was collected, purified by flash chromatography (eluting system: ethyl acetate), and recrystallized from the appropriate solvent (Table 3).

4-Amino-1-(β-hydroxyoctyl)pyrazolo[3,4-*d*]pyrimidine 12f. 4-Aminopyrazolo[3,4-*d*]pyrimidine[25] **11** (1.35 g, 10 mmol) was added under a nitrogen atmosphere to a solution of sodium (0.276 g, 12 mmol) in 25 mL of absolute ethanol. The solvent was then removed in vacuo, and the resulting sodium salt was suspended in DMF. 1,2-Epoxyoctane (1.83 mL, 12 mmol) was added dropwise, and the reaction mixture was stirred at 100 °C for 20 h. After cooling, the reaction mixture was concentrated in vacuo and the residue was treated with ice−water. The resulting solid was collected, purified by recrystallization, and characterized as a racemic mixture (Table 3).

4-Amino-1-(2-keto-3-nonyl)pyrazolo[3,4-*d*]pyrimidine 12g. 4-Aminopyrazolo[3,4-*d*]pyrimidine[25] **11** (1.35 g, 10 mmol) was added under a nitrogen atmosphere to a solution of sodium (0.276 g, 12 mmol) in 25 mL of absolute ethanol. The solvent was then removed in vacuo, and the resulting sodium salt was suspended in DMF. 3-Bromononan-2-one[24] (2.65 g, 12 mmol) was added dropwise, and the reaction mixture was stirred at 100 °C for 24 h. After cooling, the reaction mixture was concentrated in vacuo and the residue was diluted with ice−water. The resulting solid was collected and purified by flash chromatography (eluting system: ethyl acetate/methanol 9/1) to obtain **12g** as a pale yellow crystalline solid, which was characterized as a racemic mixture (Table 3).

4-Amino-1-(2-hydroxy-3-nonyl)pyrazolo[3,4-*d*]pyrimidine 12h. $NaBH_4$ (1.13 g, 30 mmol) was added portionwise to an ice-cooled solution of **12g** (2.75 g, 10 mmol) in 30 mL of methanol, while maintaining the pH between 5 and 6 by adding glacial acetic acid. Once addition was complete, stirring was continued at room temperature for 24 h. The reaction mixture was then concentrated in vacuo, and the residue was neutralized with saturated $NaHCO_3$ solution and extracted with chloroform. The combined organic extracts were dried, filtered, and evaporated to dryness under reduced pressure. The resulting oily product was purified by flash chromatography (eluting system: ethyl acetate) to obtain the target compound **12h** as a pure oily product, which was characterized as a diastereomeric mixture (Table 3).

4-Amino-1-(β-hydroxyethyl)pyrazolo[3,4-*d*]pyrimidine 12i. A suspension of 5-amino-1-(β-hydroxyethyl)-4-pyrazolecarbonitrile[26] **10** (1.52 g, 10 mmol) in 3 mL of formamide was vigorously boiled under stirring for 2 h. The cooled solution was then diluted with ice−water, and the solid separated was filtrated, washed with water, and recrystallized (Table 3).

4-Amino-2-decyl-6-phenylpyrazolo[3,4-*d*]pyrimidine 13. A mixture of 3-amino-1-decyl-4-pyrazolecarbonitrile **2e** (2.48 g, 10 mmol), benzonitrile (2.04 mL, 20 mmol), and potassium *tert*-butoxide (0.561 g, 5 mmol) was mixed thoroughly in a glass tube, then placed in an alumina bath inside the MW oven and irradiated twice at the 50% power level for 1.5 min, with a 2 min cooling period after the first irradiation cycle to avoid overheating of the reactants. The average temperature at the end of the reaction was 120 °C. After cooling, water was added to the reaction mixture and the resulting solid was collected and purified by flash chromatography (eluting system: ethyl acetate/cyclohexane 5/5) to obtain crude **13** as a white solid, which was purified by recrystallization (Table 2).

2. Biology. 2.1. Matherials and Methods. Adenosine deaminase (ADA) type IX from bovine spleen (150−200 U/mg) and adenosine were from Sigma Chemical Co. All other chemicals were of reagent grade.

2.2. Enzymatic Assay. The activity of the test enzyme was determined spectrophotometrically by monitoring for 2 min the change in absorbance at 262 nm, which is due to the deamination of adenosine catalyzed by ADA. The change in adenosine concentration/min was determined using a Beckman DU-64 kinetics software program (Solf Pack TM Module). ADA activity was assayed at 30 °C in a reaction mixture containing 50 mM adenosine, 50 mM potassium phosphate buffer pH = 7.2, and 0.3 nM enzyme solution in a total volume of 500 μL. The inhibitory activity of the newly synthesized compounds was assayed by adding 100 μL of the inhibitor solution to the reaction mixture described above. All the inhibitors were dissolved in water, and the solubility was facilitated by using DMSO, whose concentraction never exceeded 4% in the final reaction mixture. To correct for the nonenzymatic changing in adenosine concentration and the absorption by the test compounds, a reference blank containing all the above assay components except the substrate were prepared. The inhibitory effect of the new derivatives was routinely estimated at a concentration of 10^{-5} M. Those compounds found to be active were tested at additional concentrations between 10^{-5} and 10^{-11} M. Each inhibitor concentration was tested in triplicate and the determination of the IC_{50} values was performed by using linear regression analysis of the log-dose response curve. The K_i values were calculated from IC_{50}s by using the Cheng and Prusoff equation.[35]

2.3. Receptor Binding Assays. A_1, A_{2A}, and A_3 Receptor Binding. Compounds were tested for their ability to displace the specific binding of [^{3}H]DPCPX (111 Ci/mmol) from A_1ARs in bovine cerebral cortical membranes, [^{3}H]CGS21680 (47 Ci/mmol) from A_{2A}ARs in bovine striatal membranes, and [^{125}I]AB-MECA (2000 Ci/mmol) from A_3ARs in bovine cerebral

cortical membranes in the presence of the A_1AR selective antagonist DPCPX (20 nM) as described elsewhere.[36]

Compounds were dissolved in DMSO and added to the assay mixture (DMSO concentration maximum 2%). Blank experiments were carried out to determine the effect of solvent on binding. Protein estimation was based on a reported method,[37] after solubilization with 0.75 N sodium hydroxide, using bovine serum albumin as standard.

The experiments ($n = 4$), carried out in triplicate, were analyzed by an iterative curve-fitting procedure (GraphPad, Prism program, San Diego, CA).

3. Computational Chemistry. Molecular modeling and graphics manipulations were performed using the SYBYL software package,[38] running it on a Silicon Graphics R12000 workstation. Model building and conformational analysis of **3e**, (*R*)-**3k**, and (*S*)-**3k** were accomplished with the TRIPOS force field[39] available within SYBYL. Point charges of these inhibitors were calculated using the semiempirical quantum mechanics AM1 method[40] implemented in the MOPAC program.[41] Energy minimizations and molecular dynamics simulations of the ADA/**3e** complex were realized by employing the AMBER program,[42,43] selecting the all-atom Cornell et al. force field.[44]

3.1. Docking Simulations. Docking was performed with version 3.05 of the program AutoDock.[30] It combines a rapid energy evaluation through precalculated grids of affinity potentials with a variety of search algorithms to find suitable binding positions for a ligand on a given protein. While the protein is required to be rigid, the program allows torsional flexibility in the ligand.

Docking to ADA was carried out using the empirical free energy function and the Lamarckian genetic algorithm, applying a standard protocol, with an initial population of 50 randomly placed individuals, a maximum number of 1.5×10^6 energy evaluations, a mutation rate of 0.02, a crossover rate of 0.80, and an elitism value of 1. Proportional selection was used, where the average of the worst energy was calculated over a window of the previous 10 generations. For the local search, the so-called pseudo-Solis and Wets algorithm was applied using a maximum of 300 iterations per local search. The probability of performing a local search on an individual in the population was 0.06, and the maximum number of consecutive successes or failures before doubling or halving the local search step size was 4.

Fifty independent docking runs were carried out for each ligand. Results differing by less than 1.5 Å in positional root mean-square deviation (rmsd) were clustered together and represented by the result with the most favorable free energy of binding.

3.2. Ligand Setup. Molecular models of (+)-EHNA, **3e**, (*R*)-**3k**, and (*S*)-**3k** were constructed using standard bond lengths and bond angles of the SYBYL fragment library. Geometry optimizations were realized with the SYBYL/MAXIMIN2 minimizer by applying the BFGS (Broyden, Fletcher, Goldfarb, and Shannon) algorithm[45] and setting an rms gradient of the forces acting on each atom of 0.05 kcal/mol Å as the convergence criterion.

Atomic charges were assigned using the Gasteiger−Marsili formalism,[46] which is the type of atomic charge used in calibrating the AutoDock empirical free energy function. Finally, the compounds were set up for docking with the help of AutoTors, the main purpose of which is to define the torsional degrees of freedom to be considered during the docking process. The number of flexible torsions defined for each ligand is as follows: 10 in (+)-EHNA, 10 in **3e**, and 11 in both (*R*)-**3k** and (*S*)-**3k**.

3.3. Protein Setup. The crystal structure of ADA in complex with HDPR (entry code: 2ADA),[29] recovered from Brookhaven Protein Database,[47] was used. The structures were set up for docking as follows: polar hydrogens were added using the PROTONATE utility.[30] To optimize the hydrogen positions, the structures were subjected to a short energy minimization using the SANDER module of AMBER, in accordance with the type of force field and protein charges of the AutoDock empirical free energy function. Solvation parameters were added to the final protein file using the ADDSOL utility of AutoDock3.5.

The grid maps representing the proteins in the actual docking process were calculated with AutoGrid. The grids (one for each atom type in the ligand, plus one for electrostatic interactions) were chosen to be sufficiently large to include not only the active site but also significant portions of the surrounding surface. The dimensions of the grids were thus 30 Å × 30 Å × 30 Å, with a spacing of 0.375 Å between the grid points.

3.4. Molecular Dynamics Simulations. A nonbonded model was employed to treat the zinc ion, with a formal charge of 2+. The Lennard−Jones parameters of the zinc ion were adapted from Stote and Karplus.[48] The parameters of **3e** were set consistently with the Cornell et al. force field;[44] missing bond and angle parameters were assigned on the basis of analogy with known parameters in the database and calibrated to reproduce the AM1 optimized geometry. The complex was solvated by the addition of 340 TIP3P water molecules[49] within 20 Å of the catalytic zinc ion. Ten sodium ions were added as counterions to neutralize the system. The water molecules and counterions alone were energy-minimized (20 000 cycles or 0.1 kcal/mol rms deviation in energy) and equilibrated for 5 ps in a constant temperature (300 K) bath. The entire system was then subjected to SANDER energy minimization (<0.01 kcal/mol rms deviation) followed by a 200 ps MD run. During the simulation the positional constraints on the protein backbone were gradually reduced from 5 to 0.1 kcal $Å^{-2}$ mol^{-1}. The SHAKE option was used to constrain bonds involving hydrogen. A 1 fs time step was used along with a nonbonded cutoff of 8 Å at 1 atm of constant pressure. The temperature was maintained at 300 K using the Berendsen algorithm[50] with a coupling constant of 0.2 ps. Four snapshots, extracted every 25 ps from the last 100 ps MD simulation, proved to be very similar in terms of rms deviation. An average structure was calculated from the last 100 ps trajectory, and the energy was minimized using the steepest descent and conjugate gradient methods available within the SANDER module of AMBER. The CARNAL module of AMBER was used to check some structural properties (rmsd, hydrogen bonds). The hydrogen bond criterion was a maximum donor−acceptor distance of 3.5 Å and a minimum donor-proton-acceptor angle of 120°.

Supporting Information Available: Spectral data of compounds **2**−**4**, **12**, and **13** and analytical data of compounds **2**−**4**, **6**−**9**, **12**, and **13** are available free of charge via the Internet at http://pubs.acs.org.

References

(1) Cristalli, G.; Costanzi, S.; Lambertucci, C.; Lupidi, G.; Vittori, S.; Volpini, R.; Campioni, E. Adenosine Deaminase: Functional Implications and Different Classes of Inhibitors. *Med. Res. Rev.* **2001**, *21*, 105−128.

(2) Cohen, A.; Hirschhorn, R.; Horowiz, S. D.; Rubistein, A.; Polmar, S. K.; Hong, R.; Martin, D. W., Jr. Deoxyadenosine Triphosphate as a Potential Toxic Metabolite in Adenosine Deaminase Deficiency. *Proc. Natl. Acad. Sci. U.S.A.* **1978**, *75*, 472−476.

(3) Martin, D. W.; Gelfand, E. W. Biochemistry of Diseases of Immunodevelopment. *Annu. Rev. Biochem.* **1981**, *50*, 845−877.

(4) Resta, R.; Thompson, L. F. SCID: the Role of Adenosine Deaminase Deficiency. *Immunol. Today* **1997**, *18*, 371−374.

(5) Glazer, R. I. Adenosine Deaminase Inhibitors: their Role in Chemotherapy and Immunosuppression. *Cancer Chemother. Pharmacol.* **1980**, *4*, 227−235.

(6) Cha, S.; Agarwal, R. P.; Parks, R. E., Jr. Tight-Binding Inhibitors. II. Non-Steady-State Nature of Inhibition of Milk Xanthine Oxidase by Allopurinol and Alloxanthine and of Human Erythrocytic Adenosine Deaminase by Coformycin. *Biochem. Pharmacol.* **1975**, *24*, 2187−2197.

(7) Agarwal, R. P.; Spector, T.; Parks, R. E., Jr. Tight-Binding Inhibitors. IV. Inhibition of Adenosine Deaminase by Various Inhibitors. *Biochem. Pharmacol.* **1977**, *26*, 359−367.

(8) LePage, G. A.; Worth, I. S.; Kimball, A. P. Enhancement of the Antitumor Activity of Arabinofuranosyladenine by 2′-Deoxycoformicin. *Cancer Res.* **1976**, *36*, 1481−1485.

(9) Adamson, R. H.; Zaharevitz, D. W.; Johns, D. G. Enhancement of the Biological Activity of Adenosine Analogues by the Adenosine Deaminase Inhibitor 2′-Deoxycoformycin. *Pharmacology* **1977**, *15*, 84−89.
(10) Hebb, M. O.; White, T. D. Co-administration of Adenosine Kinase and Deaminase Inhibitors Produces Supra-additive Potentiation of *N*-methyl-D-aspartate-evoked Adenosine Formation in Cortex. *Eur. J. Pharmacol.* **1998**, *344*, 121−125.
(11) Poon, A.; Saynok, J. Antinociceptive and Antiinflammatory Properties of an Adenosine Kinase Inhibitor and an Adenosine Deaminase Inhibitor. *Eur. J. Pharmacol*. **1999**, *384*, 123−138.
(12) Zhu, Q.; Chen, S.; Zou, C. Protective Effects of an Adenosine Deaminase Inhibitor on Ischemia-Reperfusion Injury in Isolated Perfused Rat Heart. *Am. J. Physiol*. **1990**, *259*, 835−838.
(13) Sandhu, G. S.; Burrier, A. C.; Janero, D. R. Adenosine Deaminase Inhibitors Attenuate Injury and Preserve Energy Balance in Isolated Guinea Pig Heart. *Am. J. Physiol*. **1993**, *262*, 1249−1256.
(14) Schaeffer, H. J.; Schwender, C. F. Enzyme Inhibitors. 26. Bridging Hydrophobic and Hydrophilic Regions on Adenosine Deaminase with Some 9-(2-hydroxy-3-alkyl)adenines. *J. Med. Chem.* **1974**, *17*, 6−8.
(15) Poulsen, S. A.; Quinn, R. J. Synthesis and Structure−Activity Relationship of Pyrazolo[3,4-*d*]pyrimidines: Potent and Selective Adenosine A_1 Receptor Antagonists. *J. Med. Chem*. **1996**, *39*, 4156−4161.
(16) Chebib, M.; Quinn, R. J. 1-Phenylpyrazolo[3, 4-*d*]pyrimidines as Adenosine Antagonists: the Effects of Substituents at C4 and C6. *Bioorg. Med. Chem*. **1997**, *5*, 311−322.
(17) Chebib, M.; McKeveney, D.; Quinn, R. J. 1-Phenylpyrazolo[3,4-*d*]pyrimidines; Structure−Activity Relationships for C6 Substituents at A_1 and A_{2A} Adenosine Receptors. *Bioorg. Med. Chem.* **2000**, *8*, 2581−2590.
(18) Cottam, H. B.; Wasson, D. B.; Shih, H. C.; Raychaudhuri, A.; Di Pasquale, G.; Carson, D. A. New Adenosine Kinase Inhibitors with Oral Antiinflammatory Activity: Synthesis and Biological Evaluation. *J. Med. Chem.* **1993**, *36*, 3424−3430.
(19) Traxel, P.; Bold, G.; Frei, J.; Lang, M.; Lyndon, N.; Mett, H.; Buchdunger, E.; Meyer, T.; Mueller, M.; Furet, P. Use of a Pharmacophore Model for the Design of EGF−R Tyrosine Kinase Inhibitors: 4-(Phenylamino)pyrazolo[3,4-*d*]pyrimidines. *J. Med. Chem*. **1997**, *40*, 3601−3613.
(20) Cowar, M.; Bennett, M. J.; Kerwin, J. F., Jr. Synthesis of Novel Carbocyclic Adenosine Analogues as Inhibitors of Adenosine Kinase. *J. Org. Chem*. **1999**, *64*, 2240−2249.
(21) Biagi, G.; Giorgi, I.; Livi, O.; Pacchini, F.; Rum, P.; Scartoni, V.; Costa, B.; Mazzoni, M. R.; Giusti, L. *Erythro-* and *Threo*-2-hydroxynonyl Substituted 2-Phenyladenines and 2-Phenyl-8-azaadenines: Ligands for A_1 Adenosine Receptors and Adenosine Deaminase. *Il Farmaco* **2002**, *57*, 221−233.
(22) Schaeffer, H. J.; Vince, R. Enzyme Inhibitors. VI. Studies on the Bulk Tolerance of Adenosine Deaminase for 6-Substituted Amino-9-(3-hydroxypropyl)purines. *J. Med. Chem*. **1965**, *8*, 33−35.
(23) Wolfender, R.; Kaufman, J.; Macon, J. B. Ring-Modified Substrates of Adenosine Deaminases. *Biochemistry* **1969**, *8*, 2412−2415.
(24) Cristalli, G.; Eleuteri, A.; Volpini, R.; Vittori, S.; Campioni, E.; Lupidi, G. Adenosine Deaminase Inhibitors: Synthesis and Structure−Activity Relationships of 2-Hydroxy-3-nonyl Derivatives of Azoles. *J. Med. Chem.* **1994**, *37*, 201−205.
(25) Robins, R. K. Potential Purine Antagonists. I. Synthesis of Some 4,6-Substituted Pyrazolo[3,4-*d*]pyrimidines. *J. Am. Chem. Soc*. **1956**, *78*, 784−787.
(26) Baraldi, P. G.; Cacciari, B.; Spalluto, G.; Pineta de las Infantas y Villatoro, M. J.; Zocchi, C.; Dionisotti, S.; Ongini, E. Pyrazolo-[4,3-*e*]-1,2,4-triazolo[1, 5-*c*]pyrimidine Derivatives: Potent and Selective A_{2A} Adenosine Antagonists. *J. Med. Chem*. **1996**, *39*, 1164−1171.
(27) Taylor, E. C.; Borron, A. L. The Reaction of Nitriles with o-Aminonitriles: a Convenient Synthesis of Fused 4-Aminopyrimidines. *J. Am. Chem. Soc*. **1961**, *26*, 4967−4974.
(28) Baker, B. R.; Kozma, J. A. Irreversible Enzyme Inhibitors. CXXV. Active-Site-Directed Irreversible Inhibitors of Xanthine Oxidase Derived from Arylpurines and Pyrazolo[3,4-*d*]pyrimidines Bearing a Terminal Sulfonyl Fluoride. *J. Am. Chem. Soc*. **1968**, *11*, 656−661.
(29) Wilson, D. K.; Rudolph, F. B.; Quiocho, F. A. Atomic Structure of Adenosine Deaminase Complexed with a Transition State Analog: Understanding Catalysis and Immunodeficiency Mutations. *Science* **1991**, *252*, 1278−1284.
(30) Morris, G. M.; Goodsell, D. S.; Halliday, R. S.; Huey, R.; Hart, W. E.; Belew, R. K.; Olson, A. J. Automated Docking Using a Lamarckian Genetic Algorithm and an Empirical Binding Free Energy Function. *J. Comput. Chem.* **1998**, *19*, 1639−1662.
(31) (a) Lybrand, T. P. Ligand-Protein Docking and Rational Drug Design. *Curr. Opin. Struct. Biol.* **1995**, *5*, 224−228. (b) Bamborough, P.; Cohen, F. E. Modeling Protein-Ligand Complexes. *Curr. Opin. Struct. Biol.* **1996**, *6*, 236−241. (c) Lengauer, T.; Rarey, M. Computational Methods for Biomolecular Docking. *Curr. Opin. Struct. Biol.* **1996**, *6*, 402−406. (d) Clark, D. E.; Murray, C. W.; Lin, J. Current Issues in De Novo Molecular Design. In *Reviews in Computational Chemistry;* Lipkowitz, K. B., Boyd, D. B., Eds.; Wiley-VCH: New York, 1997; Vol. 11, pp 67−125. (e) Murcko, M. A. Recent Advances in Ligand Design Methods. In *Reviews in Computational Chemistry;* Lipkowitz, K. B., Boyd, D. B., Eds.; Wiley-VCH: New York, 1997; Vol. 11, pp 1−66.
(32) Kinoshita, T.; Nishio, N.; Nakanishi, I.; Sato, A.; Fujii, T. Crystal Structure of Bovine Adenosine Deaminase Complexed with 6-Hydroxyl-1,6-dihydropurine Riboside. *Acta Crystallogr. D* **2003**, *59*, 299−303.
(33) (a) Schaeffer, H. J. Design and Evaluation of Enzyme Inhibitors, Especially of Adenosine Deaminase. *Top. Med. Chem*. **1972**, *3*, 1−24. (b) Harriman, G. C. B.; Poirot, A. F.; Abushanab, E.; Midgett, R. M.; Stoeckler, J. D. Adenosine Deaminase Inhibitors. Synthesis and Biological Evaluation of C1′ and Nor-C1′ Derivatives of (+)-*erythro*-9-(2(*S*)-hydroxy-3(*R*)-nonyl)adenine. *J. Med. Chem.* **1992**, *35*, 4180−4184. (c) Harriman, G. C. B.; Abushanab, E.; Stoeckler, J. D. Adenosine Deaminase Inhibitors. Synthesis and Biological Evaluation of 4-Amino-1-(2(*S*)-hydroxy-3(*R*)-nonyl)-1*H*-imidazo[4,5-*c*]pyridine (3-Deaza-(+)-EHNA) and Certain C1′ Derivatives. *J. Med. Chem*. **1994**, *37*, 305−308.
(34) Chattopadhyay, S.; Mamdapur, V. R.; Chadha, M. S. Synthesis of Both the Enantiomers of 4-Dodecanolide, the Pheromone of the Rove Beetle. *Tetrahedron* **1990**, *46*, 3667−3672.
(35) Cheng, Y. C.; Prusoff, W. H. Relation between inhibition constant K_i and the concentration of inhibitor which causes fifty percent inhibition (IC_{50}) of an enzymatic reaction. *Biochem Pharmacol*. **1973**, *22*, 3099−3108.
(36) Da Settimo, F.; Primofiore, G.; Taliani, S.; Marini, A. M.; La Motta, C.; Novellino, E.; Greco, G.; Lavecchia, A.; Trincavelli, L.; Martini, C. 3-Aryl[1,2,4]triazino[4,3-a]benzimidazol-4(10*H*)-ones: A New Class of Selective A_1 Adenosine Receptor Antagonists. *J. Med. Chem.* **2001**, *44*, 316−327.
(37) Lowry, O. H.; Rosebrough, N. J.; Farr, A. L.; Randall, R. J. Protein Measurement With the Folin Phenol Reagent. *J. Biol. Chem*. **1951**, *193*, 265−275.
(38) *SYBYL Molecular Modelling System*, version 6.9.1; Tripos Inc.: St. Louis, MO, 2003.
(39) Vinter, J. G.; Davis, A.; Saunders, M. R. Strategic Approaches to Drug Design. 1. An Integrated Software Framework for Molecular Modelling. *J. Comput.-Aided Mol. Des.* **1987**, *1*, 31−55.
(40) Dewar, M. J. S.; Zoebisch, E. G.; Healy, E. F.; Stewart, J. J. P. AM1: A New General Purpose Mechanical Molecular Model. *J. Am. Chem. Soc.* **1985**, *107*, 3902−3909.
(41) MOPAC (version 6.0) is available from Quantum Chemistry Program Exchange, No. 455.
(42) Pearlman, D. A.; Case, D. A.; Caldwell, J. W.; Ross, W. S.; Cheatham, T. E., III; Debolt, S.; Ferguson, D. M.; Seibel, G. L.; Kollman, P. A. AMBER, a Package of Computer Programs for Applying Molecular Mechanics, Normal Mode Analysis, Molecular Dynamics and Free Energy Calculations To Simulate the Structural and Energetic Properties of Molecules. *Comput. Phys. Commun.* **1995**, *91*, 1−41.
(43) Pearlman, D. A.; Case, D. A.; Caldwell, J. W.; Ross, W. S.; Cheatham, T. E., III; Ferguson, D. M.; Seibel, G.; Singh, U. C.; Weiner, P. K.; Kollman, P. A. *AMBER*, version 4.1; Department of Pharmaceutical Chemistry, University of California: San Francisco, CA, 1995.
(44) Cornell, W. D.; Cieplak, P.; Bayly, C. I.; Gould, I. R.; Merz, K. M.; Ferguson, D. M.; Spellmeyer, D. C.; Fox, T.; Caldwell, J. W.; Kollman, P. A. A Second Generation Force Field for the Simulation of Proteins, Nucleic Acids, and Organic Molecules. *J. Am. Chem. Soc.* **1995**, *117*, 5179−5197.
(45) Head, J.; Zerner, M. C. A Broyden-Fletcher-Goldfarb-Shannon Optimization Procedure for Molecular Geometries. *Chem. Phys. Lett.* **1985**, *122*, 264−274.
(46) Gasteiger, J.; Marsili, M. Iterative Partial Equilization of Orbital Electronegativity − A Rapid Access to Atomic Charges. *Tetrahedron* **1980**, *36*, 3219−3228.
(47) Bernstein, F. C.; Koetzle, T. F.; Williams, G. J. B.; Meyer, E. F., Jr.; Brice, M. D.; Rodgers, J. R.; Kennard, O.; Shimanouchi, T.; Tasumi, T. The Protein Data Bank: A Computer Based Archival File for Macromolecular Structures. *J. Mol. Biol.* **1977**, *112*, 535−542.
(48) Stote, R. H.; Karplus, M. Zinc Binding in Proteins and Solution: A Simple but Accurate Nonbonded Representation. *Proteins: Struct., Funct. and Genet.* **1995**, *23*, 12−31.
(49) Jorgensen, W. L.; Chandrasekhar, J.; Madura, J. D.; Impey, R. W.; Klein, M. L. Comparison of Simple Potential Functions for Simulating Liquid Water. *J. Chem. Phys.* **1983**, *79*, 926−935.

(50) Berendsen, H. J. C.; Postma, J. P. M.; van Gunsteren, W. F.; DiNola, A.; Haak, J. R. Molecular Dynamics with Coupling to an External Bath. *J. Chem. Phys.* **1984**, *81*, 3684−3690.
(51) Chakrabarti, J. K.; Hotten, T. M.; Pullar, I. A.; Tye, N. C. Synthesis and Pharmacological Evaluation of a Series of 4-Piperazinylpyrazolo[3,4-*b*]- and -[4, 3-*b*][1, 5]benzodiazepines as Potential Anxiolytics. *J. Med. Chem.* **1989**, *32*, 2573−2582.
(52) Baraldi, P. G.; Cacciari, B.; Spalluto, G.; Pineda de las infantas y Villatoro, M. J.; Zocchi, C.; Dionisotti, S.; Ongini, E. Pyrazolo-[4,3-*e*]-1,2,4-triazolo[1,5-*c*]pyrimidine derivatives: potent and selective A_{2A} adenosine antagonists. *J. Med. Chem*. **1996**, *39*, 1164−1171.
(53) Kelly, J. L.; Davis, R. G.; McLean, E. W.; Glen, R. C.; Soroko, F. E.; Cooper, B. R. Synthesis and Anticonvulsivant Activity of N−Benzylpyrrolo[2,3-*d*]-pyrazolo[3,4-*d*]-, and -triazolo[4,5-*d*]-pyrimidines: Imidazole Ring-Modified Analogues of 9-(2-Fluorobenzyl)-6-(methylamino)-9*H*-purine. *J. Med. Chem*. **1995**, *38*, 3884−3888.
(54) Cheng, C. C.; Robins, R. K. Potential Purine Antagonists. VI. Synthesis of 1-Alkyl-and 1-Aryl-4-substituted Pyrazolo[3, 4-*d*]-pyrimidines. *J. Org. Chem*. **1956**, *21*, 1240−1256.

JM050136D